8-2021

Effect of Radiation on Bond Behavior Between Concrete and Steel Bar: Development of Experimental Protocol

Mohammed Abdelrahman
University of Tennessee, Knoxville, mabdelr4@vols.utk.edu

To the Graduate Council:

I am submitting herewith a thesis written by Mohammed Abdelrahman entitled "Effect of Radiation on Bond Behavior Between Concrete and Steel Bar: Development of Experimental Protocol." I have examined the final electronic copy of this thesis for form and content and recommend that it be accepted in partial fulfillment of the requirements for the degree of Master of Science, with a major in Civil Engineering.

Z. John Ma, Major Professor

We have read this thesis and recommend its acceptance:

Timothy James Truster, Mark Denavit

Accepted for the Council:
Dixie L. Thompson

Vice Provost and Dean of the Graduate School

(Original signatures are on file with official student records.)

Effect of Radiation on Bond Behavior Between Concrete and Steel Bar: Development of Experimental Protocol

A Thesis Presented for the

Master of Science

Degree

The University of Tennessee, Knoxville

Mohammed Abdelrahman Salih Abdelrahman

August 2021

To my lovely family

and friends

Acknowledgments

I would like to express my gratitude to my parents (Najwa and Abdelrahman), my wife Areej, my daughter Julie, sisters, and brother for their never-ending prayers, encouragement, and guidance throughout my life. They provide me with power, motivation, and self-assurance.

I am in great debts to the The University of Tennessee, Knoxville, and Oak Ridge National Laboratory for providing me the financial support and world class facilities which made my life smoother and easier to devote myself fully to academic and research works.

I would like to express my heartfelt gratitude to Prof. Z. John Ma, my thesis advisor, for his invaluable support, guidance, constant encouragement, and all possible cooperation and patience throughout the course of my research and thesis documentation preparation. Working with him was a wonderful and educational experience that I greatly appreciated.

My sincere thanks and appreciation are due to the thesis committee members Dr. Timothy J. Truster and Dr. Mark D. Denavit for investing their time and their support, critical reviews and suggestions to improve this work.

I am thankful to all of the Civil and Environmental Engineering Department's faculty and staff, as well as my colleagues and friends, for their assistance during the road.

Abstract

There is a need to assess the effect of radiation on the behavior of bond strength between steel reinforcement and concrete. However, there is geometrical constraints in the cylindrical capsule which limit the size of concrete samples. Thus, developing a protocol to produce pullout sample and a test setup is needed.

A protocol for fabricating high-precision concrete samples with embedded #2 steel bar has been developed based on the results of an experimental program. A pullout system has also been developed to investigate the bond activity of concrete and steel. This research looks at two different aggregate sizes 3/8 inch (10 mm) and 1/2 inch (13 mm).

The compressive strength, bond stress, and slip values for concrete with a maximum aggregate size of 1/2 inch (13 mm) are higher than those for concrete with a maximum aggregate size of 3/8 (10 mm), according to the results. Future research should look into the impact of maximum aggregate size on bond activity.

Table of Contents

List of Tables

List of Figures

Chapter 1

Introduction

Concrete is the most widely used construction material in the world. It is used in many applications, such as building frames, tanks, bridges and pavements. Annually, more than 10 billion tons of concretes are consumed all over the world (Grosse, 2007).

Also, there are hundreds of nuclear reactors all over the world. In nuclear power plants, safety of reinforced concrete structures is vital to humankind.

Researchers examined the impact of neutrons, gammarays, and the resulting heating and drying processes on concrete power, as well as their underlying mechanisms, and confirmed the concrete degradation mechanism due to neutron irradiation. Metamictization of rock-forming minerals is the primary cause of degradation, which contributes to aggregate expansion (Maruyama et al., 2017).

There is a need to assess the effect of irradiation on the behavior of bond strength between steel reinforcement and concrete. However, due to geometrical constraints in the cylindrical capsule special concrete samples are needed. Also, developing a protocol to produce those samples is needed.

1.1 Specimen size

In their work, pre-irradiation experiments were carried out to determine the best test specimen size for limiting gamma heating (Maruyama et al., 2017). The pre-irradiation experiments were performed on mortar specimens 2×4 in (50×100 mm). The specimen's

core temperature was about 181 °F (83 °C), while its surface temperature was about 136 °F (58 °C), which is the same as the temperature of the reactor's cooling water. The surface and core of the 50 mm specimen differ by 45 °F (26 °C). Assuming the tensile strength of 0.58 ksi (4 MPa) and a Young's modulus of 2900 ksi (20 GPa) for normal concrete, cracks begin to appear if tensile strain reached to 200 μ. If a thermal expansion coefficient of 6.7 μ/°F (10 μ/°C) is assumed, cracks could form in the concrete at the surface. Therefore, it was decided to minimize the core–surface temperature differential such that the corresponding strain differential was kept below 200 μ. In Figure 1.1, the appearance of cracks caused by a large coresurface temperature difference was greatly reduced by limiting the specimen diameter to 1.57 in (40 mm). As a result, 1.57 in (40 mm) specimens were chosen for testing to reduce the confusing effects of gamma heating over a broad internal temperature distribution.

1.2 Capsule

The experiment on concrete in nuclear plant carried out inside a capsule designed specially for this purpose.

A double tube of aluminum makes up the capsule (Figure 1.2). The cylinder contains cement paste and concrete specimens, which are separated from the cooling water to provide some clearance. Cooling water comes in through the bottom of the outer cylinder and exits through the tip. This design allows cooling water to flow between the outer surface of the inner cylinder and the inner surface of the outer cylinder This design allows cooling water to flow between the inner cylinder's outer surface and the outer cylinder's inner surface, eliminating the heat produced in the specimens. To collect the gas and water vapor produced by radiation, a tube connects the inner cylinder to a measuring device outside the reactor. A helium-based flushing device is installed in the tube to remove any clogs.

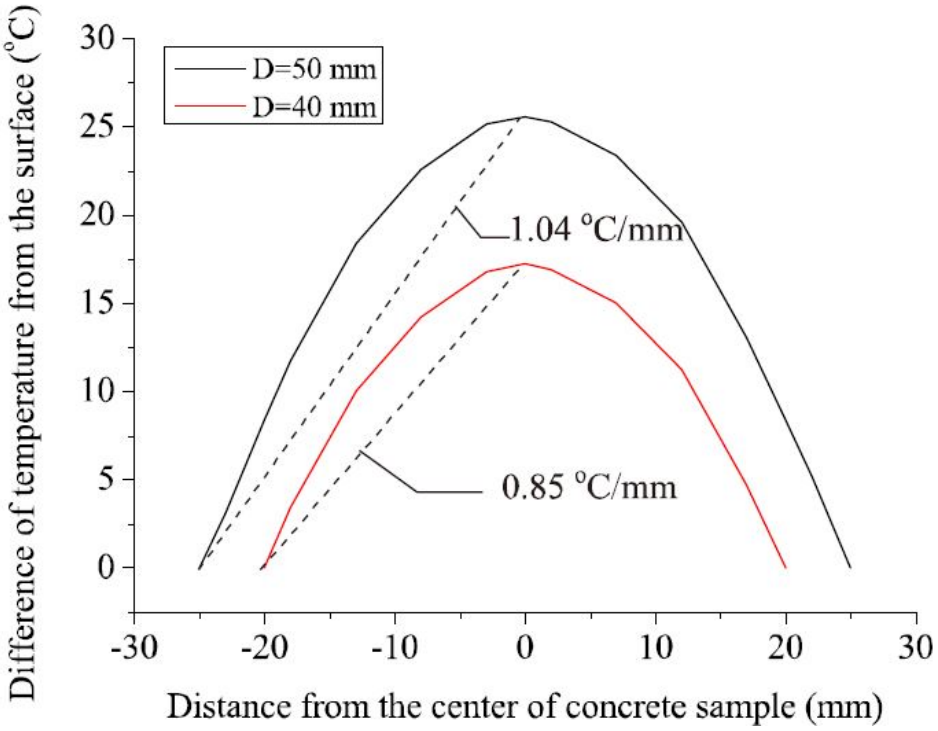

Figure 1.1: Calculated temperature distribution in concrete specimen with dimension of 50 mm and 40 mm

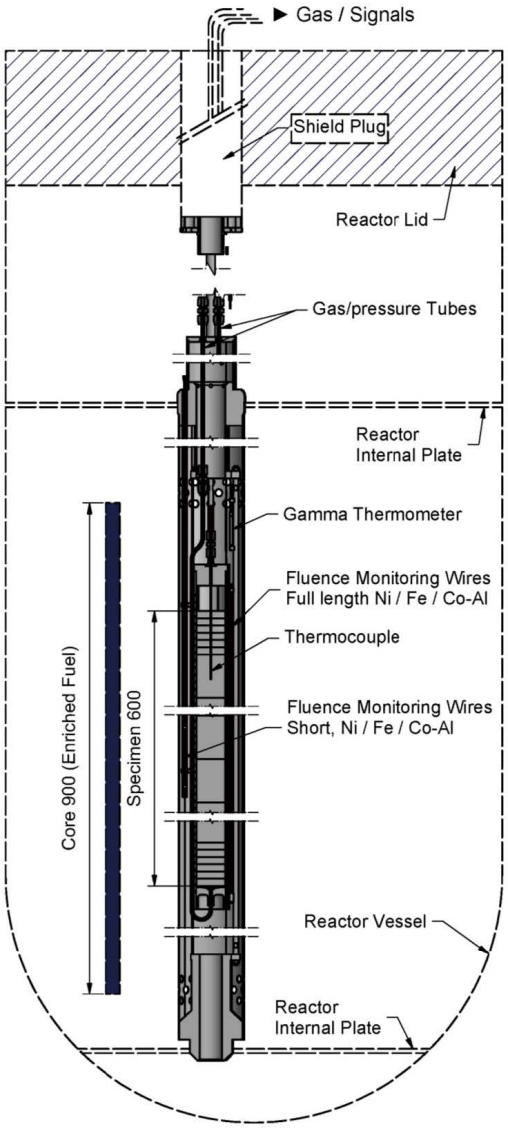

Figure 1.2: Schematic of specimens capsule and their monitoring set-up

1.3 Objectives

The overall objectives of this study are to develop a protocol to fabricate high precision samples and to design a pullout system in order to study bond behavior. The specific objectives are as the following:

1. To develop a protocol to mix, cast and cure concrete
2. To develop a protocol to perform a pullout test
3. To evaluate the mechanical properties of the concrete
4. Conduct pullout tests and analyze results

Chapter 2

Literature Review

2.1 Bond Force

ACI Committee 408 (2003) defines the term bond force as "the force that tends to move a reinforcing bar parallel to its length with respect to the surrounding concrete. Bond strength represents the maximum bond force that may be sustained by a bar."

For a deformed bar, there are three mechanisms assisting bond force transformed from the reinforcement to the surrounding concrete (Figure 2.1): The first one is the chemical adhesion between the bar and the concrete; the second one is the frictional force arising from the roughness of the interface; and the third one is the mechanical anchorage or bearing of the ribs against the concrete surface (ACI Committee 408, 2003).

2.2 Factors affecting bond

Structural characteristics, bar properties, and concrete properties can all influence bond.

The structural characteristics include concrete cover, bar spacing, the bonded length of the bar, the degree of transverse reinforcement, the bar casting position, and the use of noncontact lap splices. The bar properties include bar size and geometry, steel stress and yield strength, and bar surface condition, while the concrete properties include compressive strength, tensile strength and fracture energy, aggregate type and quantity,

concrete slump and workability, and the effects of admixtures, fiber reinforcement, and degree of consolidation.

Bond strength increases as cover and bar spacing increase. The mode of failure also depends on cover and bar spacing (Rehm and Eligehausen, 1979). For large cover and bar spacing, it is possible to obtain a pullout failure and avoid splitting failure. For smaller cover and bar spacing, a splitting tensile failure occurs resulting in lower bond strength (ACI Committee 408, 2003).

For a given development length and degree of confinement; the larger bars achieve higher total bond forces than smaller bars (Darwin et al., 1992). However, the bond force is not proportional to the area and increases more slowly than the bar area, which means that a longer embedment length is needed for a larger bar to fully develop a given bar stress (Rehm and Eligehausen, 1979). The pullout test of deformed bars achieve a higher bond resistance than plain bars. For epoxy-coated bars under all conditions of confinement, bond strength increases with relative rib area (Darwin et al., 1995). The bond strength of steel that yield is slightly different that steel does not yield for a given bonded length (Darwin et al., 1995).

The bond force-slip response of reinforcing bars is a function of their relative rib area (ratio of bearing to shearing area), not the precise combination of rib height and rib spacing. The initial stiffness of load-slip curves increases with an increase in relative rib area under all conditions of bar confinement. Bond strength is independent of deformation pattern under conditions of relatively low confinement, where bond strength is controlled by concrete splitting. Bond strength increases when additional bar confinement is created by transverse reinforcement or a higher cover, relative to the bond strength of bars with less confinement. As the relative rib area grows, so does the extent of the increase in bond strength (Darwin and Graham, 1993). The variations in face angle do not impact bond strength for ribs angles greater than 40 degrees, according to several researchers, since the high face angle is flattened by crushed concrete in front of the ribs (Lutz and Gergely, 1967; Skorobogatov and Edwards, 1979).

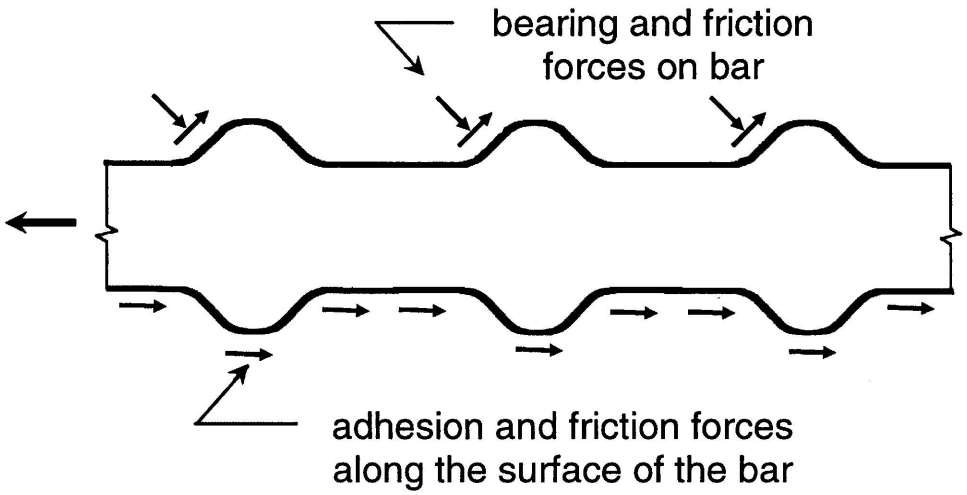

Figure 2.1: Bond force transfer mechanisms

The bond strength increase with a higher compressive up to 8 ksi (55 MPa) and the bond strength is represented using the square root of the compressive strength $\sqrt{f'_c}$. For higher strength concrete, however, the average bond strength at failure, normalized with respect to $\sqrt{f'_c}$, decreases with an increase in compressive strength (Hamad and Itani, 1998).

For bars not confined by transverse reinforcement, the higher-strength coarse aggregate increases concrete contribution to total bond force by up to 13% compared with a weaker coarse aggregate (Zuo and Darwin, 1998). Properly consolidated, low-slump concrete usually provides the best bond with reinforcing steel. This is due to the fact that concrete continues to settle and bleed after cast which leaves a void below rigidly held bars (ACI Committee 408, 2003). Also, the mode of failure depends on cover and bar spacing (Darwin et al., 1992; Orangun et al., 1977; Rehm and Eligehausen, 1979). For large cover and bar spacing, it is possible to obtain a pullout failure. For smaller cover and bar spacing, a splitting tensile failure occurs, resulting in lower bond strength.

ACI-318 and FIB- 2010 codes equations for bond strength calculation work well only when the maximum aggregate size is 12.7 mm (1/2 inch) and above. Therefore, maximum aggregate size is critical for bond strength when smaller size aggregates are used (Iqbal et al., 2018).

In the past few decades, scholars have proposed various bond stress–slip relationships and corresponding bond models. Eligehausen et al. (1982) suggested a bond model, arguing that bond strength increased as concrete strength increased, and that it could be viewed as a function of the square root of concrete compressive strength. Filippou et al. (1983) also developed an analytical model to explain the hysteresis efficiency of reinforced concrete beam–column joints in 1983. As a result, the Eligehausen–Filippou model came to be known as the Eligehausen–Filippou model which later adopted the CEB-FIP model code 2010 as shown in Figure 2.2 (Walraven et al., 2010). Using the CEB-FIP Model Code 2010's nonlinear bond stress–slip relationship as an example, if the pullout fails, the bond stress (τ) between the concrete and steel bar as a function of the relative displacement (S) can be calculated using the following equations:.

$$\tau = (\frac{S}{S_1})^{\alpha} \quad \text{for } 0 \leq S \leq S_1 \tag{2.1}$$

$$\tau = \tau_{max} \quad \text{for } S_1 \leq S \leq S_2 \tag{2.2}$$

$$\tau = \tau_{max} - \frac{(\tau_{max} - \tau_3)(S - S_2)}{(S_3 - S_2)} \quad \text{for } S_2 \leq S \leq S_3 \tag{2.3}$$

$$\tau = \tau_f \quad \text{for } S_1 > S_3 \tag{2.4}$$

where τ_{max} is the peak bond stress; τ_f is the residual bond stress; S is the bond slip; and S1, S2, and S3 are the slip at the start of peak bond stress, slip at the end of peak bond stress, and slip at the start of residual bond stress, respectively; α is a curve fitting parameter that must not be larger than one to be physically meaningful. The values of parameters S_1, S_2, S_3 α and τ_{bf} are assumed based on statistical analysis of the experimental results from the previous researches for examples (Abrishami and Mitchell, 1993; Vázquez-Herrero et al., 2013). However, the bond stress–slip relationship varied along the longitudinal axis of the steel bar and therefore need a correction by introducing position function describes the bond stiffness at different positions (Tang, 2021).

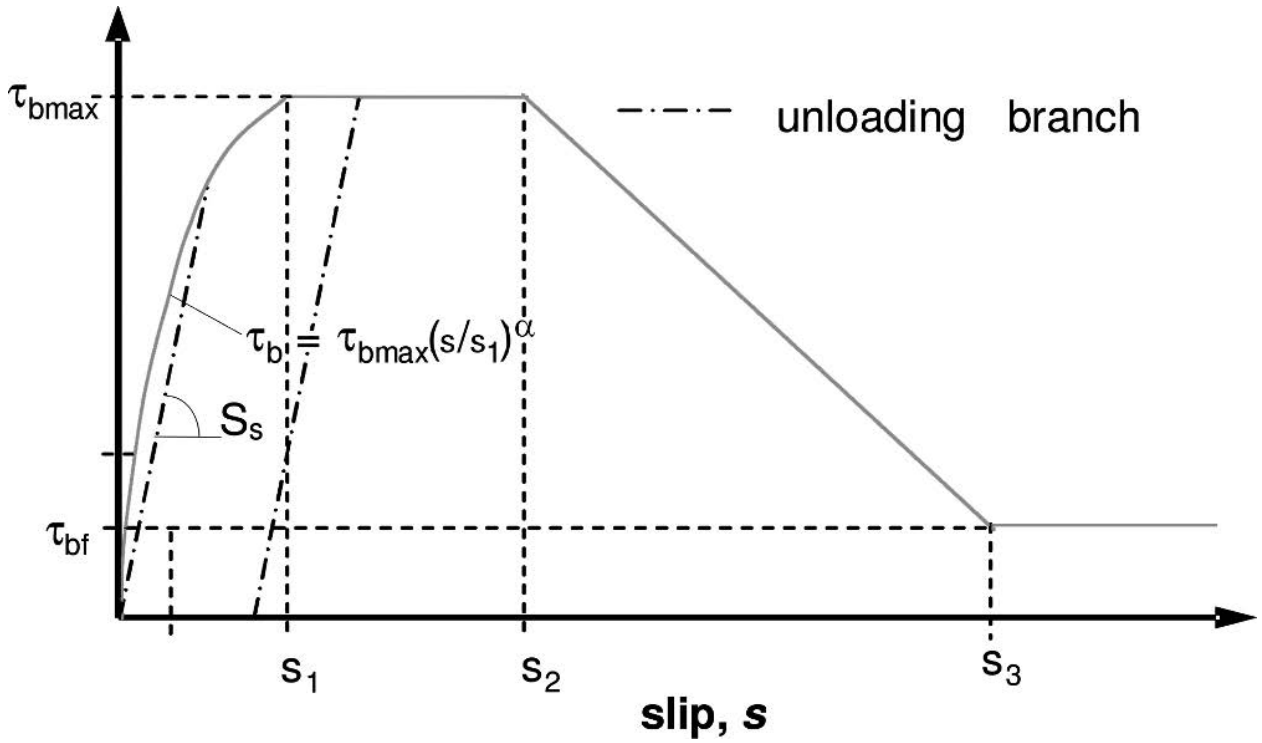

Figure 2.2: Bond stress-slip relationship

Chapter 3

Experimental Program

3.1 Introduction

In accordance with the theme of this research, the materials employed in the research program were procured from different sources in differnt countries. Further, the experimental procedures followed in the investigation are clearly laid out.

The research work was carried out in three major stages. The first stage involves selection of the materials. In the second phase, preparation of specimens was carried out and in the third phase, testing of specimens was done to ascertain the mechanical properties. In this chapter, all these three phases are discussed thoroughly.

3.2 Developing a protocol

The method that was used to develop a protocol was conducting trial mixes with a selected group of materials. Different techniques of consolidation, mold material and mold design were used to achieve an acceptable protocol before moving to the next part.

The mix design was fixed to be same as one used in a previous study "Development of soundness assessment procedure for concrete members affected by neutron and gamma-ray irradiation" (Maruyama et al., 2017).

3.2.1 Specimen details

The final concrete cylinders that are used for the pullout testing must be precisely 1.57 inch (40 mm) in diameter and 2.36 inch (60 mm) in height. The precision is need to fit the samples in the capsule since the gap between the inner surface of the capsule and outer surface of concrete will be small to few micrometer (see section 1.2). The steel rebar (#2 bar) embedded in the center is required to have a diameter of 1/4 in (6.35 mm). The maximum aggregate size is 1/2 inch (13 mm). Additionally, a manufactured aluminum mold along with PVC piping were used for the concrete molds in order to help complete effective fabrication trials in the lab.

3.2.2 Material for trial mixtures

Aggregates

A crushed granite was chosen as coarse aggregate while natural sand was used as fine aggregate for trial mix. Figure 3.1 shows the coarse and the fine aggregates used in the trial phase. The grading of coarse aggregates is shown in Table 3.1 and the fine aggregate grading is shown in Table 3.2.

Cement

Two types of cement were used to prepare trial mix. The first one is Type III low alkali cement with blaine fineness 6220 cm^2/g. This cement gives a high followability due to high surface area. However, the previous study reported low flowability due using high early-strength ordinary Portland cement (H) with blaine fineness 4340 cm^2/g. Therefore, A second type of cement was used to give a closer result. The trial using Type I cement with blaine fineness is 4530 cm^2/g gives similar behavior of fresh concrete.

(a) Coarse aggregate **(b)** Fine aggregate

Figure 3.1: Coarse and fine aggregates used in trial mix

Table 3.1: Grading of coarse aggregate used in trial mix

Nominal Dimension of Test Sieve (mm)	Grading of Aggregate (%)
2.5	1
5	4
10	76
13	99
15	100

Table 3.2: Grading of fine aggregate used in trial mix

Nominal Dimension of Test Sieve (mm)	Grading of Aggregate (%)
0.15	7
0.3	22
0.6	40
1.2	62
2.5	91
5	100

Mix design

Table 3.3 summarizes the design mix of previous study used to prepare the trial mix.

3.2.3 Results of trial mixures

As shown in Figure 3.2, the concrete was mixed using a small mixer 0.01 m^3 (0.4 ft^3) capacity and four PVC pipes were utilized for molds. Each specimen was made using a different fabrication method as shown in Table 3.4. Prior to fabricate molds, PVC pipes was cut and attached with steel plate to used as a mold as shown in Figure 3.3.

The photos obtained from the first fabrication trial, provided in Figure 3.4 , show that rodding of the specimens resulted in a poor distribution of aggregate. The steel bar and small sample sizes made it difficult for manual rodding to be effective. Additionally, the sample that was fabricated using solely the drop table had large hole and gaps where concrete and aggregate were not present. The fabrication method resulting in the best aggregate distribution form trial 1 was the sample that was tapped manually with a hammer 10 times per layer. A significant number of pores were observed on the cured samples as well.

After the first trial it was clear that a mechanical vibration is needed to reduce voids and to obtain more homogeneous concrete. A commercial dremel was modified by adding rod to vibrate the concrete (see Figure 3.5).

The second fabrication trial was conducted using a reusable aluminum mold fabricated using Computer numerical control machine (CNC) in order to ensure that the cylinders are the appropriate size and that the steel bars maintain center alignment (Figure 3.6). A vibrator was used to vibrate each concrete layer in the two molds for 15 seconds; two layers were poured to fill each mold. The lowest speed on the vibrator, speed 1, was used for this trial. The same mixer shown in Figure 3.2 was used to mix the concrete.

The photo provided in Figure 3.7 shows that the cured samples fabricated using vibration have a more even distribution of aggregate than the samples observed in trial 1. However, the lowest vibration speed may have resulted in the significant number of pours observed in the photo.

Table 3.3: Design of trial mix

Concrete type	Water (kg/m^3)	Cement (kg/m^3)	Fine Agg. (kg/m^3)	Coarse Agg. (kg/m^3)
GA	183	366	799	995

Figure 3.2: The mixer

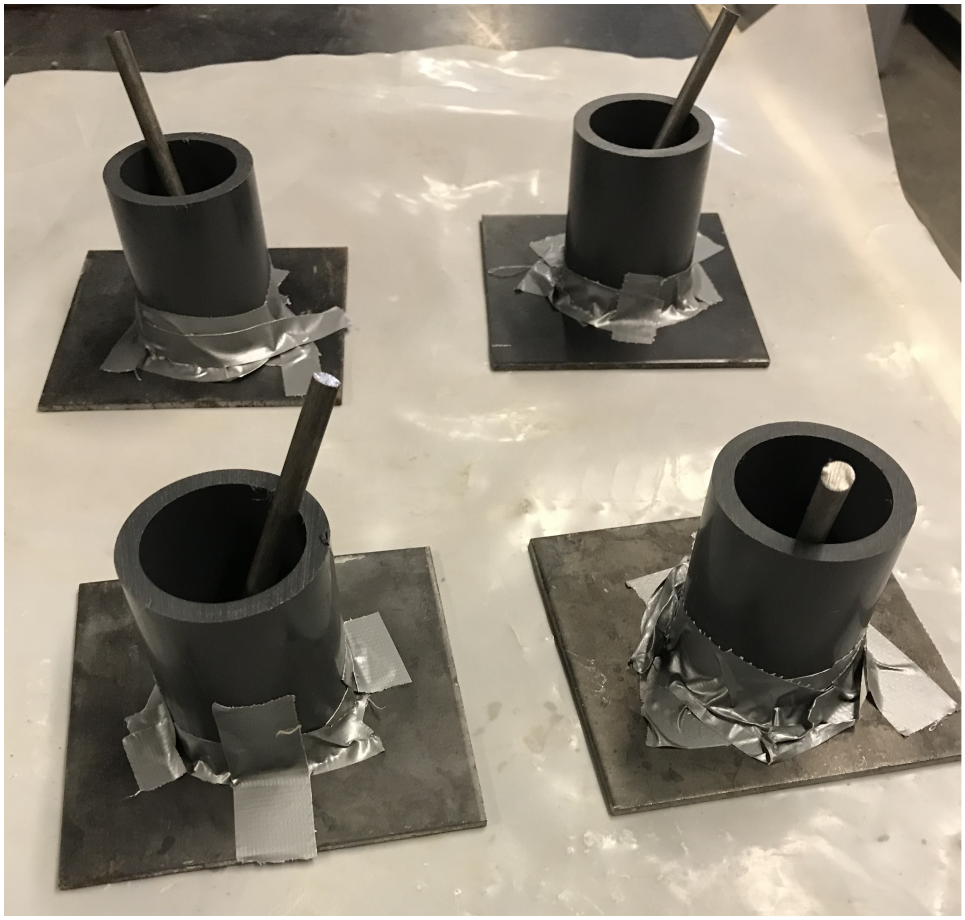

Figure 3.3: PVC pipe used as mold for the first trial

Table 3.4: The consolidations methods used in first trial

Fabrication Method	Number of Concrete Layers	Number of Roddings per Layer	Number of Rotations on Drop Table per Layer	Number of Manual Taps with Hammer per Layer
#1	2	15	10	-
#2	2	15	-	-
#3	2	-	10	-
#4	2	-	-	10

Figure 3.4: Results of first trial

Figure 3.5: The vibrator before adding a rod

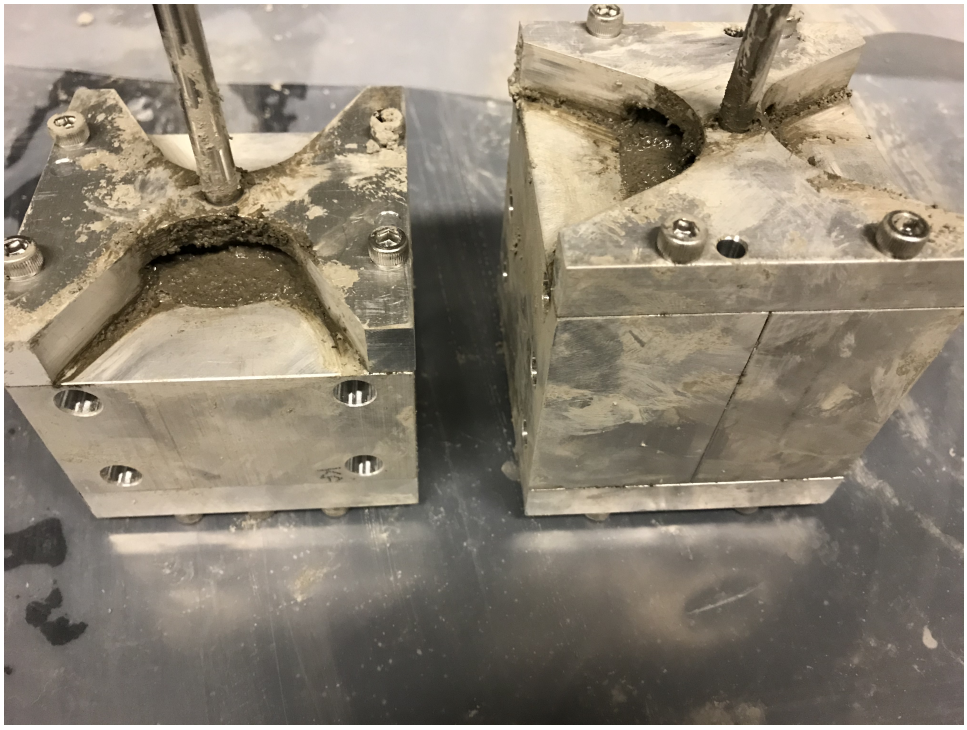

Figure 3.6: Aluminum mold

Figure 3.7: The sample of the second trial

The third fabrication trial was conducted using the same aluminum molds utilized in the second fabrication trial. Similar, to the second fabrication trial, each mold was filled with two concrete layers of even height. Each layer was vibrated for 15 seconds using the vibrator with a speed of 2, which was slightly faster that the speed used in the second trial. The concrete cylinders on the left side of the photo shown in Figure 3.8 are the samples resulting from the second fabrication trial described previously. The samples on the right side of the photo are the samples resulting from the third fabrication process.

The fabrication process used for trial 3 was similar to trial 2 except for utilizing a slightly higher vibration speed on the vibrator. Although a higher speed was used, a similar number of pores were observed in the photo provided in Figure 3.7. Additionally, the samples on the right side of the photo in Figure 3.8 are from the third trial and show signs of indentations made from concrete residue left on the molds from trial 2. The aluminum molds used in trial 2 were difficult to completely clean which resulted in some concrete being left behind. As a result, a new reusable mold was developed using CNC machine from PVC plates for further fabrication testing with the goal of minimizing concrete residue left behind after cleaning; this mold is shown in Figure 3.9 below.

The fourth fabrication trial was conducted to investigate the effect of speed of the vibrator on reducing the pore in concrete. Five concrete cylinders were made using five different PVC molds. Two concrete layers were poured to fill each mold, and each layer was vibrated for 15 seconds with the vibrator. As shown in Figure 3.10, the aggregate distribution was similar for the range of vibration speeds used; however, the amount and size of pores reduced gradually as the vibration speed was increased from 1 to 5.

Due to difficulty of vibrating the mold with a space constraint, it was decided to keep the vibration at speed 1 and increase the time of vibrating to 40 seconds for each layer of casting.

Last trials were conducted with the final design. Figure 3.11 shows an acceptable sample based on the developed protocol.

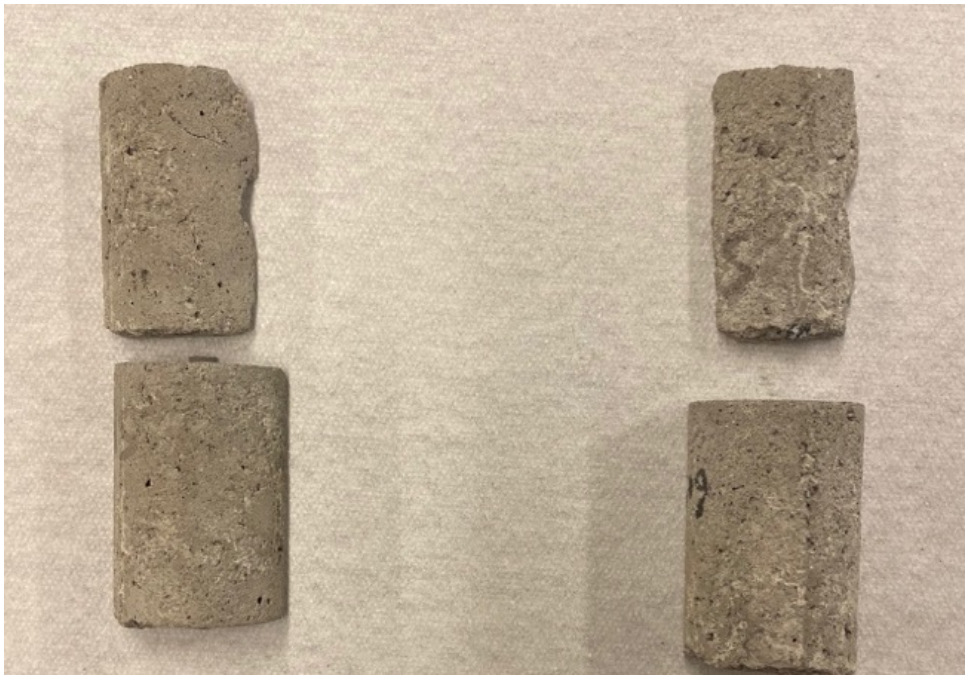

Figure 3.8: The sample of the third trial

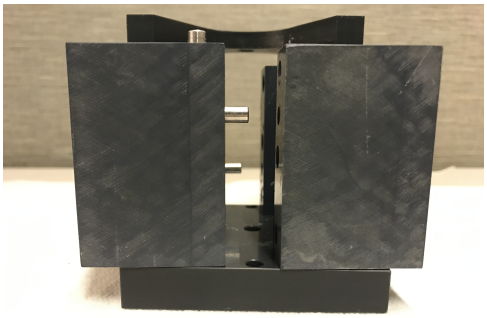

(a) Side view

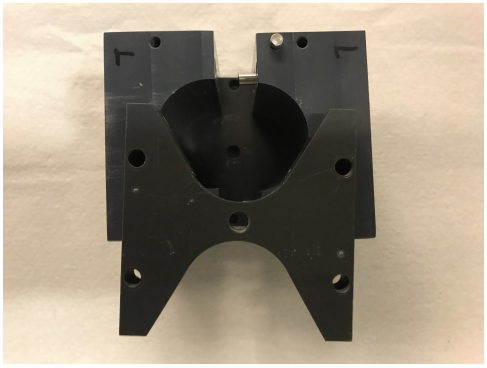

(b) Top view

Figure 3.9: PVC mold fabricated using CNC machine

Figure 3.10: The samples of the fourth trial

Figure 3.11: The sample of last trial

3.3 Materials used in the study

Materials used to fabricate final samples are discussed here.

3.3.1 Cement

High early-strength ordinary Portland cement (H) was used to prepare samples. Table 3.5 shows chemical composition of the cement.

3.3.2 Coarse aggregates

Two types of aggregates were used as coarse aggregates. The physical properties and grading are summarized in Table 3.6.

3.3.3 Fine aggregates

Crushed sandstone was used as fine aggregates. The physical properties and grading are summarized in Table 3.7.

3.3.4 Water

Distilled water was used to mix concrete.

3.3.5 Steel rebar

A special #2 rebar 1/4 inch (6.35 mm) nominal diameter was used to embed centrally in concrete. Piece of the bar shown in Figure 3.12. The average height of ribs is 0.008 inch (0.205 mm) and the distance between ribs is 0.216 inch (5.5 mm).

Table 3.5: Chemical composition of used cement. (H: high early-strength ordinary Portland cement

Cement Type	Density (g/cm^3)	Blaine value (cm^2/g)	Chemical Composition (mass%)												Total
			Ig.loss	SiO_2	Al_2O_3	Fe_2O_3	CaO	MgO	SO_3	Na_2O	K_2O	TiO_2	P_2O_5	MnO	
H	3.14	4340	1.04	20.78	4.98	2.46	65.4	1.24	3.04	0.21	0.28	0.29	0.32	0.09	100.11

Table 3.6: Coarse aggregate physical properties and grading

Coarse Aggregate	Rock Type	Density (g/cm^3)		Absorption (%)	Solid Content (%)	Grading of Aggregate (%)				
		in Saturated Surface-dry Condition	in Oven-dry Condition			Nominal Dimension of Test Sieve (mm)				
						2.5	5	10	13	15
A	Tuff	2.66	2.64	0.75	-	1	4	76	99	100
B	Sandstone	2.64	2.61	1.09	66.4	0	0	50	100	100

Table 3.7: Sand physical properties and grading

Fine Aggregate	Rock Type	Density (g/cm3)		Absorption (%)	Solid Content (%)	Grading of Aggregate (%)						
		in Saturated Surface-dry Condition	in Oven-dry Condition			Nominal Dimension of Test Sieve (mm)						
						0.15	0.3	0.6	1.2	2.5	5	10
Mountain Sand	Sandstone	2.61	2.57	1.48	68.3	7	22	40	62	91	100	100

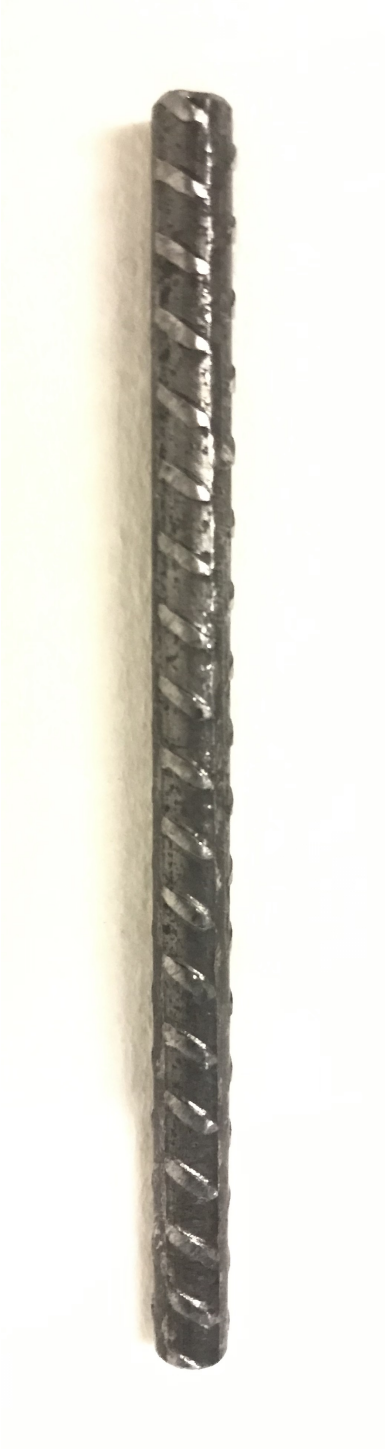

Figure 3.12: #2 rebar

3.3.6 Specimen details

The PVC molds manufactured using CNC machine was used to cast pullout samples (Figure 3.10). The diameter of each sample is 1.57 inch (40 mm) and the height is 2.36 inch (60 mm). 0.984 inch (25 mm) of steel embedded in samples are debonded from concrete using knob shown in Figure 3.13. The procedure for debonding in process of producing samples is explained in the next section. Figure 3.14 shows the specimen details. Additional samples for mechanical properties and characterization were cast using 2×4 inch cylinder (50×100 mm).

3.4 Protocol to fabricate final samples

3.4.1 Materials preparation

Sieving

All coarse and fine aggregates were sieved to the required sizes using a sieve machine. Each size was kept separately in buckets with appropriate labels. The aggregates were washed using tap water and cleaned from any dust.

Aggregates drying

Coarse and fine aggregates were placed in an oven for 24 hours at 230 °F (110 °C). After removing the materials from the oven, the aggregates were cooled down to room temperature. Then they were stored in dry buckets and sealed with plastic sheet to avoid any moisture ingress.

3.4.2 Fabrication protocol

Weighing

All the constituents of mixture were weighed using a digital balance with a precision of ±0.002 Ibs (±0.01 g).

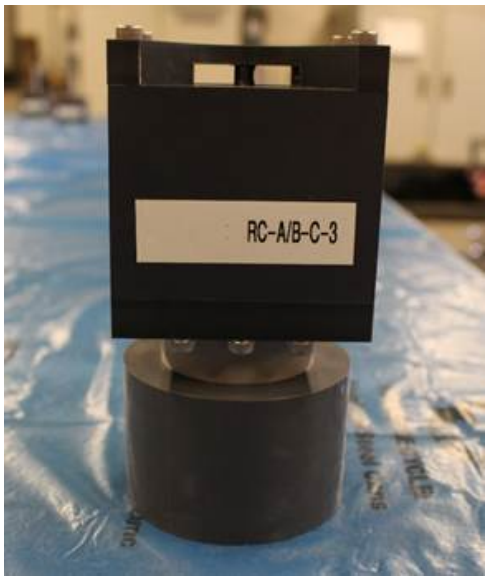

(a) Side view

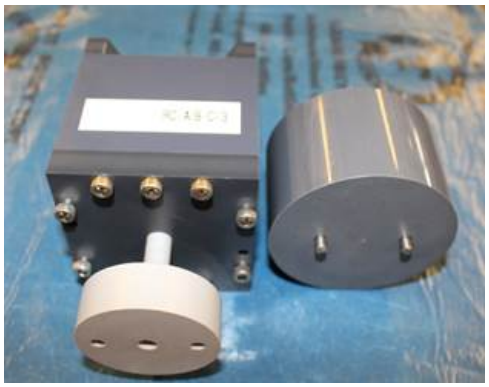

(b) Bottom view

Figure 3.13: The mold and knob

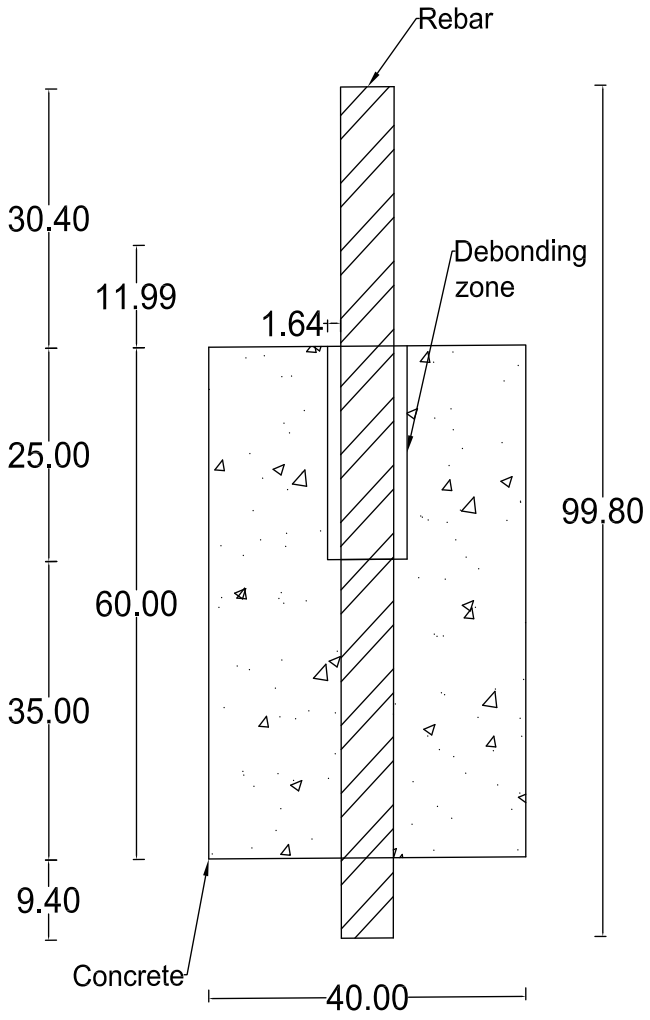

Figure 3.14: The Specimens details

Mixer preparation

The mixer part were cleaned with tap water. 20 minutes before mixing, the inside surface of the bowl and the beaters were wiped and dried with tissue paper to eliminate residual water.

Molds and rebar preparation

Molds were arranged on the table over plastic sheet to avoid any spilled materials. The rebar in the molds for pullout samples was pushed to reach the surface of plastic sheet on the table (end of the knob).

Batching concrete

All dried constituents were placed in the mixer. The mixer was covered with plastic sheet and run for one minute. Water was added gradually for 3 minutes. Mixer was run for another one minute (The total mixing time is 5 minutes).

All the molds were filled with concrete up to the top of the molds in two layers. A food spoon was used to make samples. For the other cylinders (2×4 in), scoop was used to cast concrete.

The molds was vibrated for 40 seconds (speed of the vibrator was kept on speed 1). The vibrator rod touched the bottom and sides of the molds and moved in way to reach all the internal volume of concrete. The slumped height was refilled then followed by vibration for 30 seconds. The depth of vibration rod was overlapped approximately 0.4 inch (one centimeter) with the previous slumped layer.

Thin pieces of aluminum were used to finish top surface of samples immediately after consolidation process. After casting, all equipment and tools were cleaned right away with a stiff-bristle brush and water.

Excess concrete was piled in a piece of plastic and the rinse water was disposed in the concrete cleaning area.

Early-age curing

Immediately after finishing the top surfaces, all specimens were covered with plastic sheet to minimize water loss.

After finishing the specimens, the bottom rods of the debonding knob were rotated 5 times counterclockwise and 5 times clockwise (to get the threaded part of the rods to the bottom of the mold) every 30 minutes for 8 hours.

After 8 hours, the debonding knobs of the "pull-out" molds were removed. Specimens were covered with plastic sheet to avoid evaporation.

Demolding

All the specimens were demolded after 2 days of pouring concrete. All the bolts were removed using an Allen key. The top and bottom of the molds were removed. A rubber mallet was used in case of any resistance by giving mold a gentle nudge. All the molds label in the molds were duplicated on the specimens with an anti-fade water-resistant marker. A visual inspection was carried out to assess soundness of the samples to locate surface defects in the samples.

Curing

All specimens were placed in curing tanks L×W×H= 4×2×2 ft (1.22×0.61×0.61 m) filled up to half of the height (60 gallons of lime saturated water). A certified curing tank heater was used to maintain temperature of fluid in curing tank 77 °F (25 °C).

3.5 Test on aggregates

3.5.1 Relative density (Specific Gravity)

Specific gravity was conducted for coarse and fine aggregate according to ASTM Standard C127 (2015) and ASTM Standard C128 (2015), respectively

3.5.2 Absorption

Aggregate absorption test was conducted to find excessive amount of water to be added to mixture to keep W/C ratio equal to 0.5. The test followed ASTM Standard C127 (2015) and ASTM Standard C128 (2015), respectively.

3.6 Test on final mix

In this sections, a brief description to the tests carried out in this study was presented:

3.6.1 Compressive Strength

Compressive strength specimens are 2×4 inch (50×100 mm) concrete cylinders. The compressive strength was determined according to ASTM C39/C39M (2012) after water curing. The specimens were tested using an automatic compression machine of hydraulic type of Gilsob® brand, shown in Figure 3.15. The load was applied at a constant rate of 400 Ib/s until the specimen failed and the maximum load was noted. The compressive strength was calculated by dividing the failure load by the cube cross-sectional area.

3.6.2 Pullout test

A setup was designed and manufactured to perform pullout tests. Figures 3.16 and 3.17 show schematic drawing of the setup and photo of the final design. The steel frame is set between two ball joints with ability to rotate in all directions to avoid eccentricity. Two steel pieces with teeth in diamond shape, one in L shape and the other rectangular, are used to act as gripping system by tightening four bolts (see Figure 3.18). To measure slip at free end, a plate in the middle of frame with tow holes is used to pass two sensors, one acting against steel bar and the other against the concrete surface (See Figure 3.19). Another sensor holder is attached with the gripping device to allow measuring the displacement from top (load end), as shown in Figure 3.20.

The slip for the free end was calculated by subtracting the reading of the sensor measuring against steel bar from the one that measuring the displacement against concrete cylinder.

On the load end, the measuring of displacement is against top plate with an assumption that top plate is moving as a rigid body and there is no slip between gripping device and the steel bar. An Instron® brand machine was used for pullout test. All the tests were conducted with a displacement control at the rate of 0.01575 in/min (0.4 mm/min).

3.7 Preparation of final mix

The procedures mentioned earlier were strictly followed to produce the final set. Two mixtures were prepared. The first mix Conc-A has aggregates with the maximum aggregate size of 1/2 inch (13 mm) and Conc-B has of aggregates with maximum aggregate size of 3/8 inch (10 mm). Mix design of two mixtures is summarized in Table 3.8. High early-strength ordinary Portland cement (H) and fined aggregate from crushed sandstone were used to prepare all the samples.

Figure 3.21 shows the Conc-A and Conc-B after demold. Curing in tank full with lime water took 48 and 47 days for Conc-A and Conc-B, respectively.

Figure 3.15: Gilsob® hydraulic type compressive strength testing machine.

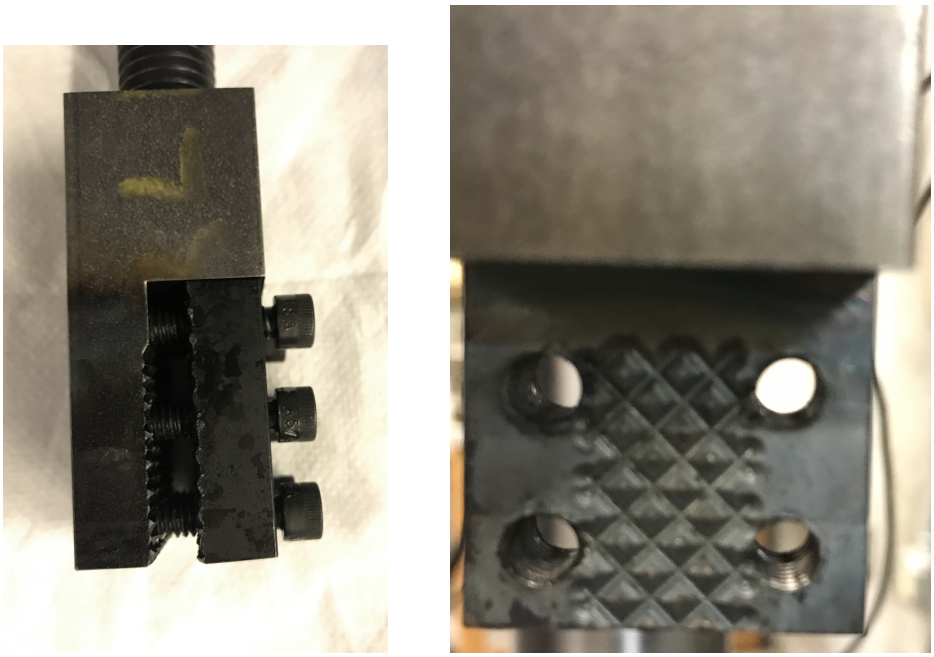

(a) Grip **(b)** Teeth of grip

Figure 3.18: Grip device of steel bar

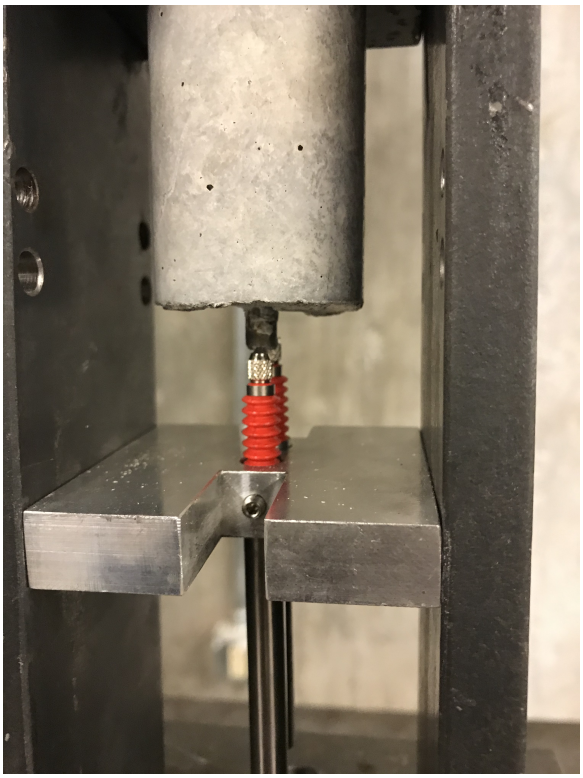

Figure 3.19: Sensors at free end

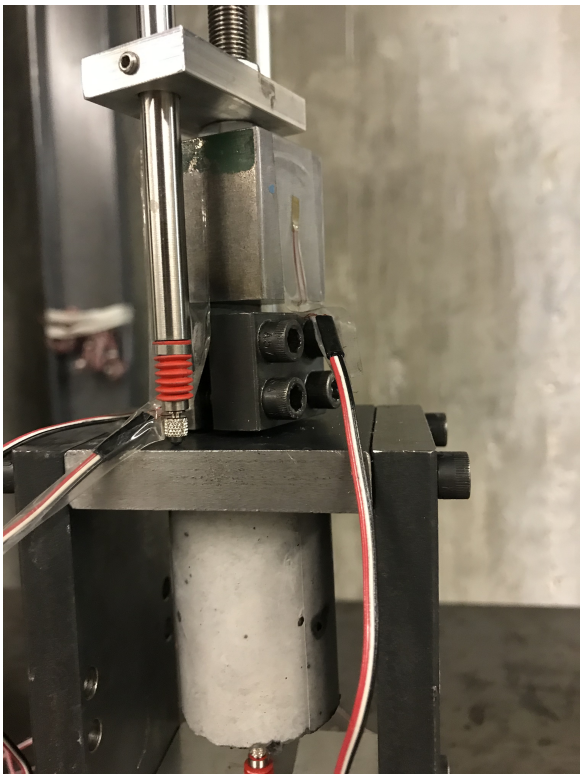

Figure 3.20: Sensor at load end

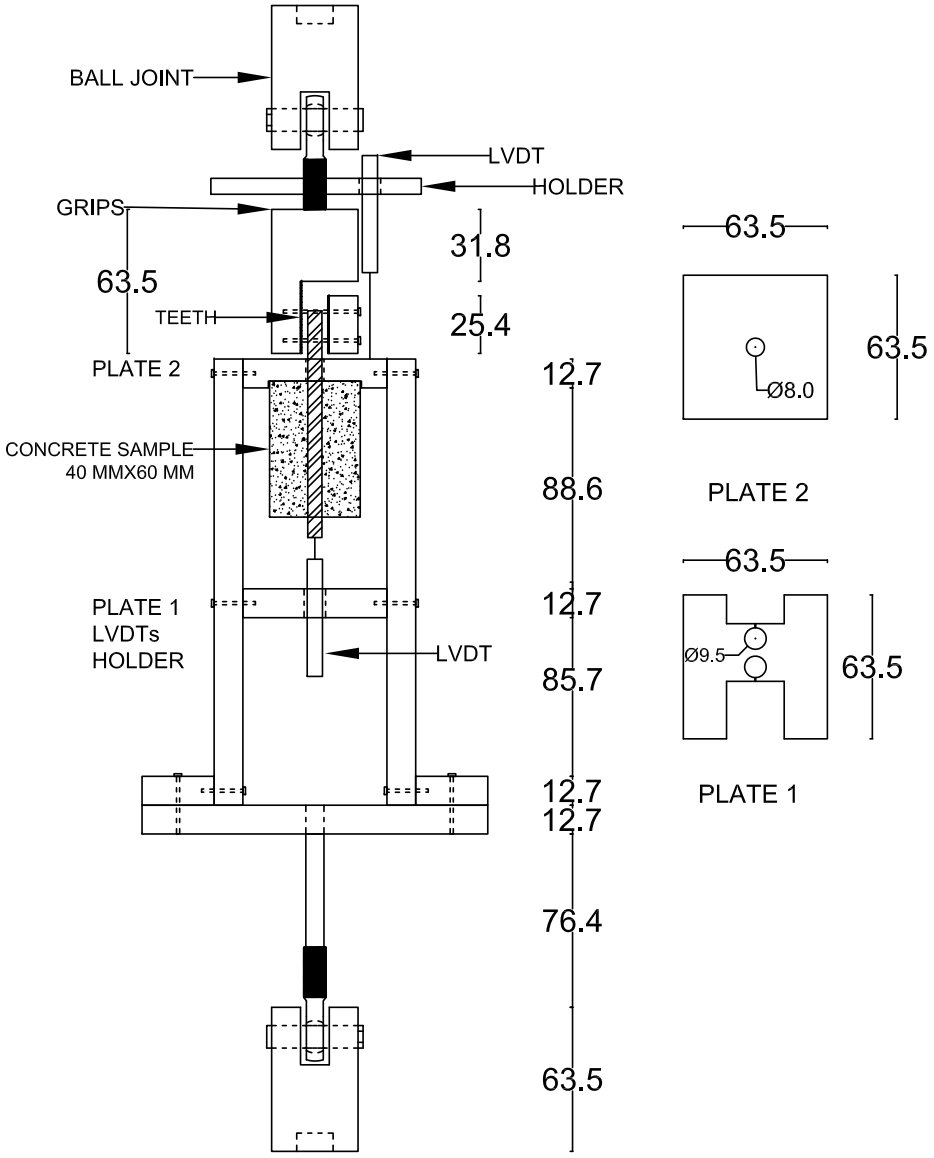

Figure 3.16: Schematic drawing of setup for pullout test

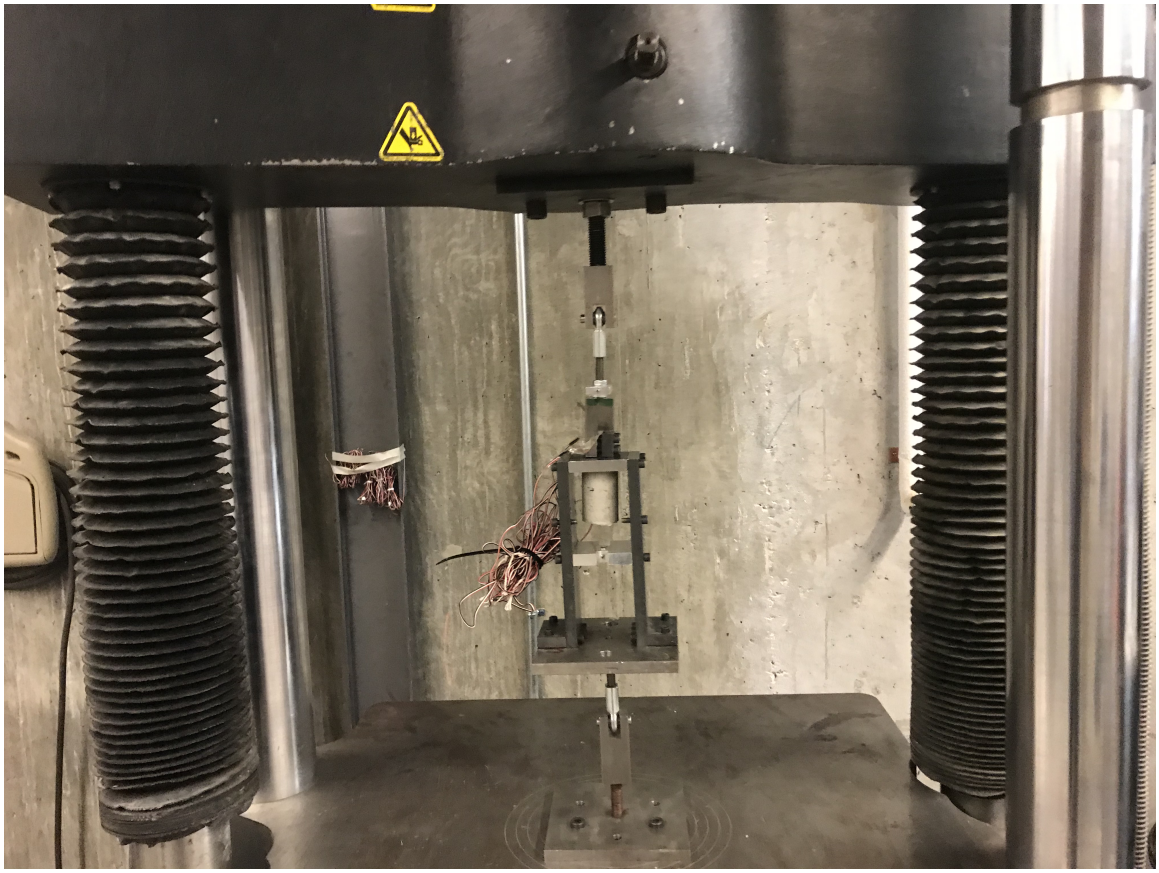

Figure 3.17: Setup for pullout test

Table 3.8: mixture proportions of concretes

Mix	Water (kg/m3)	Cement (kg/m^3)	Sand (kg/m^3)	Agg-A (kg/m^3)	Agg-B (kg/m^3)
Conc-A	183	366	799	995	-
Conc-B	177	354	757	-	1057

(a) Conc-A

(b) Conc-B

Figure 3.21: Final mix after demold

Chapter 4

Results and Discussion

In this chapter, the results of the experimental work were presented and discussed.

4.1 Compressive strength

Figure 4.1 shows a typical failure mode. Table 4.1 summarizes the compressive strength of two mixes. The mix with maximum aggregate size 13 mm (Conc-A) shows a higher compressive strength than the mix with the maximum aggregate size of 10 mm (Conc-B). This could be attributed to the fact that the first mix has more cement content (366 kg/m^3 to 354 kg/m^3 for Conc-B) as well as more content of fine aggregate (799 kg/m^3 to 757 kg/m^3); which leads to a higher compactability.

4.2 Pullout test

Table 4.2 summarizes the maximum bond stress and measured slip of two mixes.

Figures 4.2 and 4.3 show the bond-slip curve for the Conc-A-1 and Conc-A-2, while Figure 4.4 show Conc-A samples after the failure by spiting. The results of third sample could not be extracted due to machine error or malfunction. As expected, the loaded end bond force-slip curve shows a lower initial stiffness than the unloaded end curve (free end).

Table 4.1: Mix design and compressive strengths for the two mixes

Concrete	Cylinder #	Comperssive Strength [ksi (Mpa)]	Average compressive strength [ksi (Mpa)]	Standard deviation
Conc-A	cylinder 1	8.7 (59.8)	8.6 (59.3)	0.148
	cylinder 2	8.7 (59.6)		
	cylinder 3	8.4 (58.0)		
Conc-B	cylinder 1	7.3(50.5)	7.3 (50.3)	0.068
	cylinder 2	7.3 (50.0)		
	cylinder 3	7.2 (49.6)		

Figure 4.1: A compressive test after failure

Table 4.2: Pullout test results

Sampe #	Maximum bond stress [ksi (MPa)]	Slip at max [inch (mm)]
Conc-A-1	1.8 (12.3)	0.0302 (0.813)
Conc-A-2	1.8 (12.2)	0.03263 (0.829)
Conc-B-1	1.2 (8.1)	0.0121 (0.307)
Conc-B-2	1.2 (8.0)	0.0124 (0.316)
Conc-B-3	1.2 (8.0)	0.0116 (0.295)

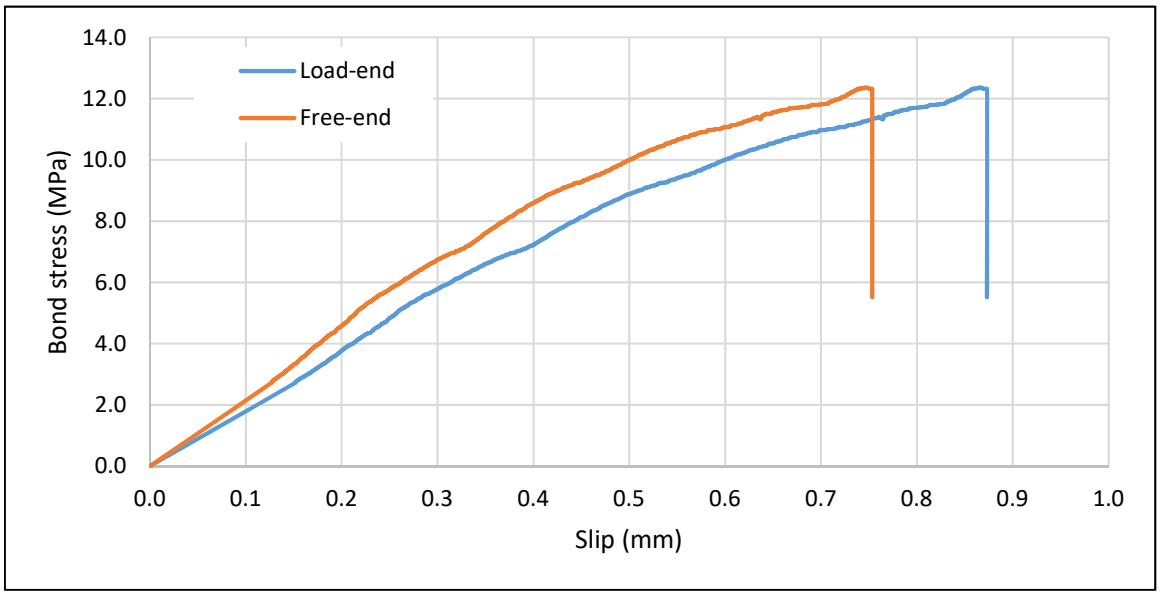

Figure 4.2: Bond-slip relationships of Conc-A-1

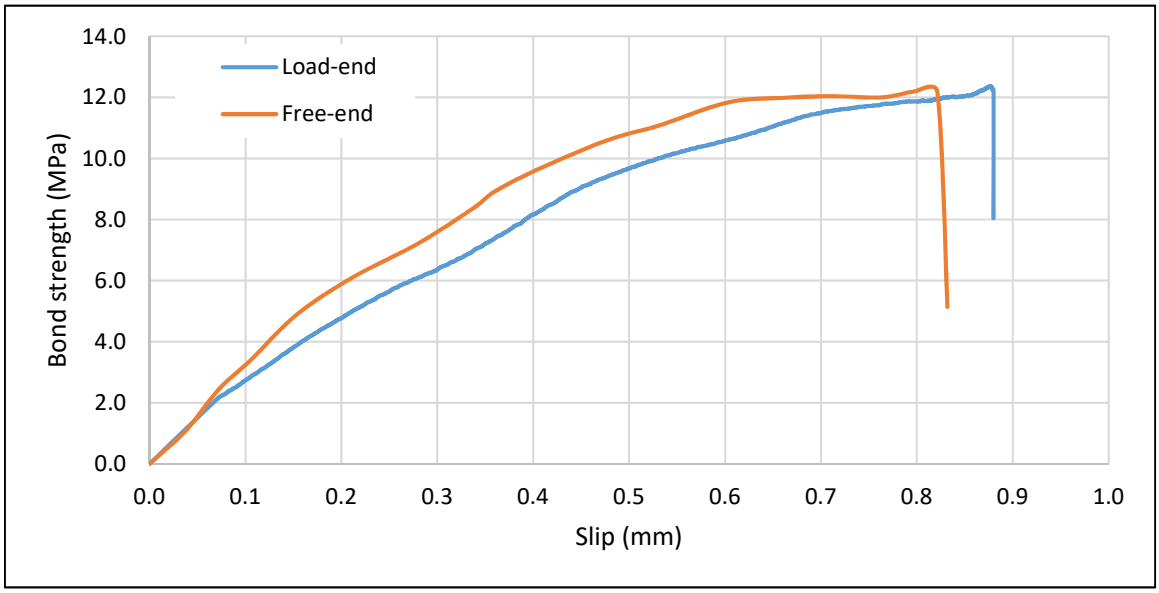

Figure 4.3: Bond-slip relationships of Conc-A-2

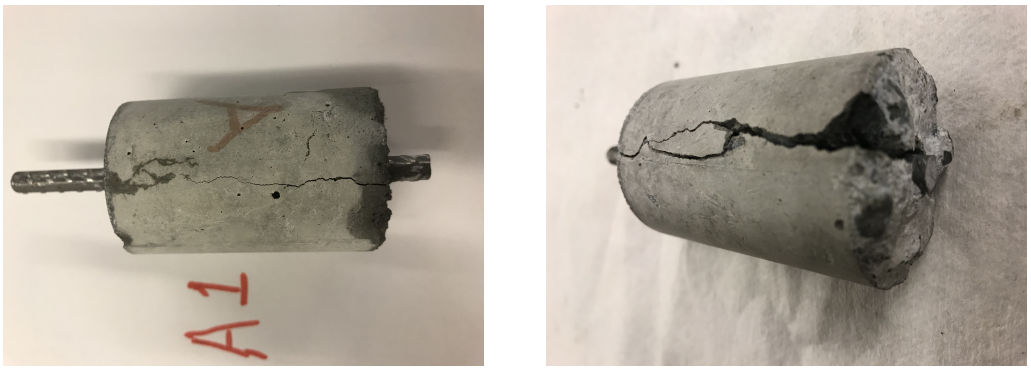

(a) Conc-A-1 **(b)** Conc-A-2

Figure 4.4: Conc-A-1 and A-2 after failure

The difference represents the lengthening of the reinforcing bar between the two points of slip measurement. Also, the steel embedded in concrete has high confinement compared to the steel at the loaded end. The maximum bond strength was 12.3 MPa (1.8 ksi) and 12.2 (1.8 ksi) for Conc-A1 and Conc-A2, respectively. The failure mode was a combination of pullout and splitting. Due to that fact, the slip reached high value taking in consideration the geometry.

Figures 4.5, 4.6 and 4.7 show the bond-slip curve for the Conc-B-1, Conc-B-2 and Conc-B-3, while Figure 4.8 shows the Conc-B samples after the failure by splitting. Again, the maximum bond strength were 8.0-8.1 MPa (1.2 ksi) for the three samples. Those results is less than Conc-A by almost 34%. This also is following the same pattern for compressive strength as mentioned earlier. However, it was noticeable that the slip is much lower than Conc-A due to sudden failure by splitting.

Figures 4.9 and 4.10 show the slip at load-end and free-end with bond stress normalized to $\sqrt{f'_c}$. The average normalization values are 1.59 and 1.13 for Conc-A and Conc-B, respectively. This indicates there is no good relationship between compressive and bond stress which in line with work of other researcher. For example Iqbal et al. (2018) found for higher strength concrete (namely 55 MPa (8 ksi)); the average bond strength at failure, normalized with respect to $\sqrt{f'_c}$, decreases with an increase in compressive strength (Hamad and Itani, 1998) while the bond stress increase with a higher Compressive up to 8 ksi.

for higher strength concrete, however, the average bond strength at failure, normalized with respect to $\sqrt{f'_c}$, decreases with an increase in compressive strength (Hamad and Itani, 1998).

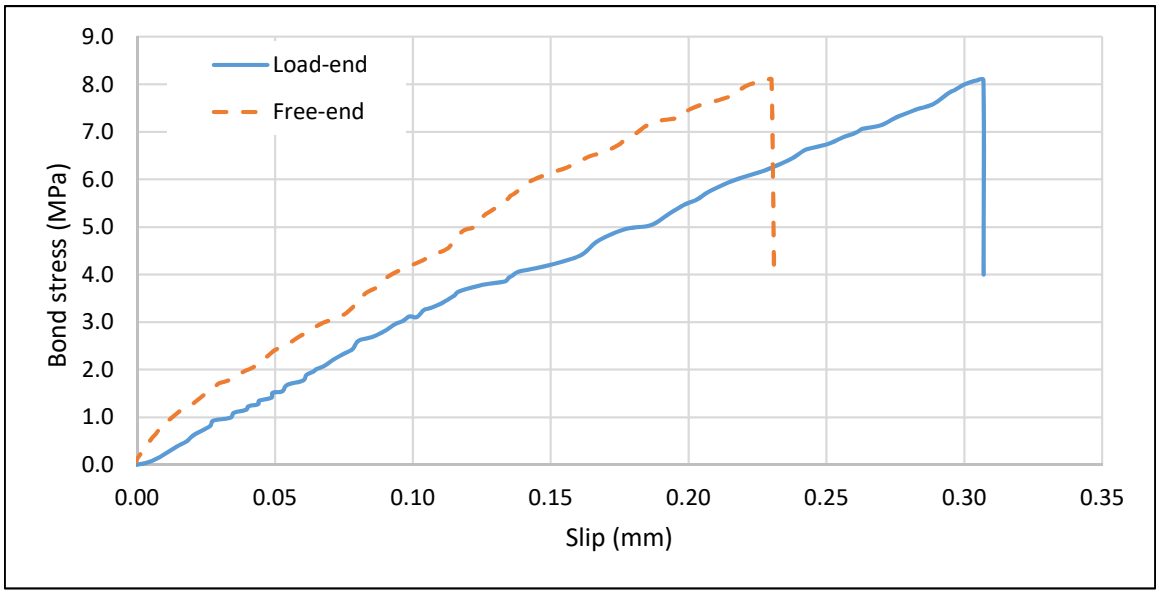

Figure 4.5: Bond-slip relationships of Conc-B-1

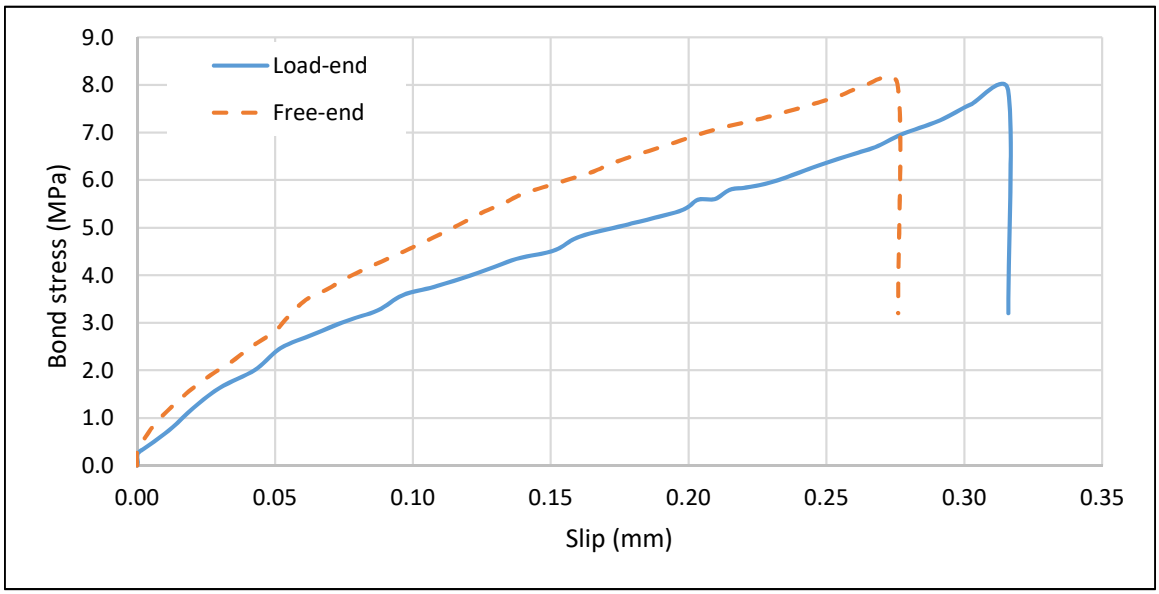

Figure 4.6: Bond-slip relationships of Conc-B-2

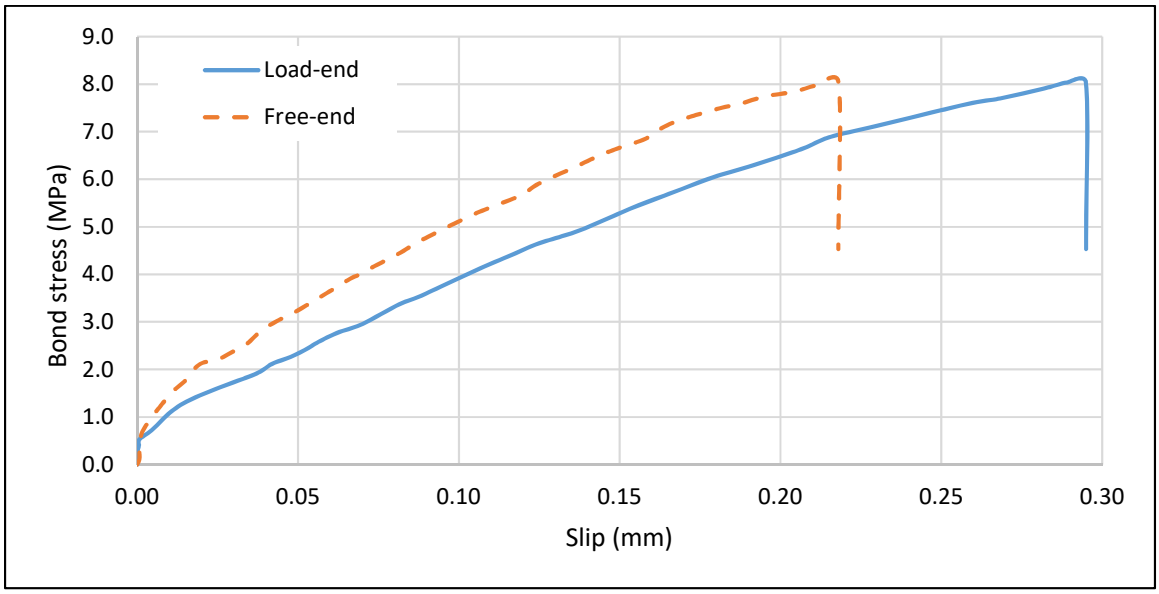

Figure 4.7: Bond-slip relationships of Conc-B-3

(a) Conc-B-1

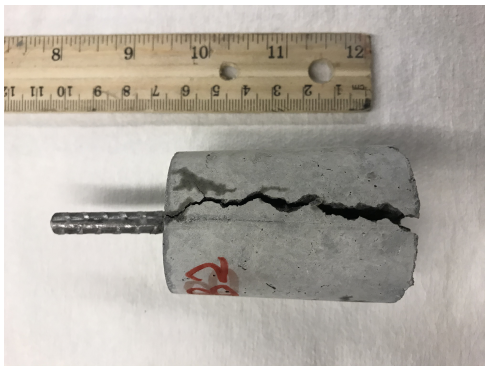

(b) Conc-B-2

(c) Conc-B-3

Figure 4.8: Conc-B-1 B-2 and B-3 after failure

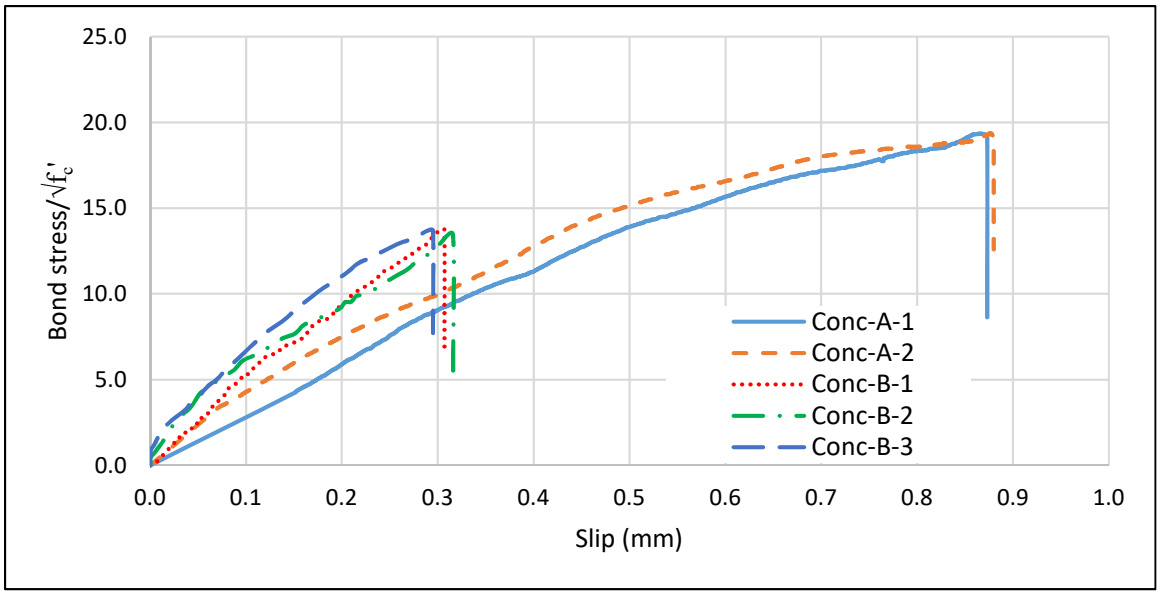

Figure 4.9: Load-end slip vs bond stress/$\sqrt{f'_c}$

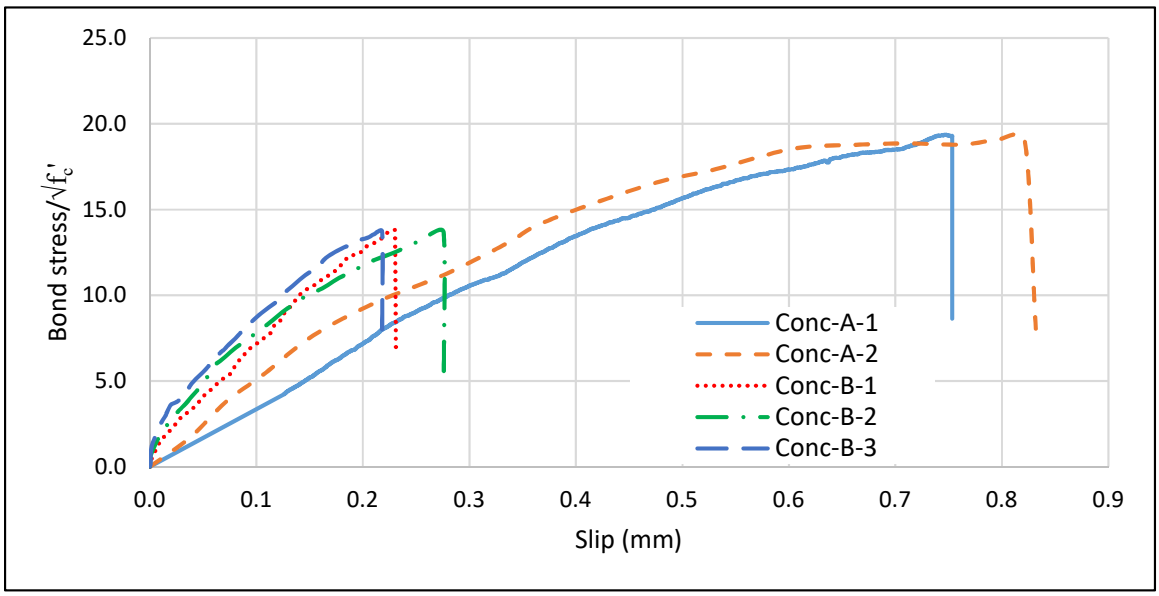

Figure 4.10: Free-end slip vs bond stress/$\sqrt{f'_c}$

Chapter 5

Conclusions and Recommendations

5.1 Conclusion

1. A protocol was developed to manufacture high precision concrete with #2 embedded steel which is partially de-bonded from concrete. The size of concrete samples were 40 mm diameter (1.57 in) and 60 mm height (2.36 in).

2. A setup for pullout test was developed and tested.

3. The compressive strength at 48 days for concrete with maximum aggregate size of 13 mm was 59.3 MPa (8.6 ksi) and at 47 days for concrete with maximum aggregate size of 10 mm was 50.3 MPa (7.3 ksi).

4. The maximum bond strength for concrete with maximum aggregate size of 13 mm was 12.3 MPa (1.8 ksi) and for concrete with maximum aggregate size of 13 mm was 8.1 MPa (1.2 ksi).

5. The failure mode for concrete with maximum aggregate size of 13 mm was a combination of pullout and splitting while it was by splitting for concrete with maximum aggregate size of 10 mm. The slip values were much higher for the first concrete compared with the second one [0.03263 in (0.829 mm) against 0.012 in (0.316 mm)].

6. There is a need to consider the effect of maximum aggregate size on bond behavior for the size less than 13 mm.

5.2 Recommendations

Scale study is needed to assess the pattern of bond stress with increasing the aggregate size. Some of the parameters to investigate are: concrete cove, rebar size and the maximum aggregate size.

1. To distinguish the irradiation effect for temperature on the small scale size used in this analysis, different treatment conditions are needed. Three identical sets can be made: one at room temperature, one at the same profile temperature of reactor, and one that senses both temperature and irradiation simultaneously in a nuclear reactor.

2. To scale up from a 1.57 inch (40 mm) specimen to a real-world situation in a nuclear power plant with walls up to 36 inches (1.4 meters), different clear covers are required, ranging from 0.7 inch (17 mm) to 1 inch (25 mm), 2 inch (50 mm), and 3 inch (75 mm).

3. A set of reinforcement steel has also be used namely #2, #4, #6 and #8.

4. A Different mix designs must also be developed to account for the maximum aggregate sizes 3/8 in (9.5 mm), 1/2 in (12.7 mm), 3/4 in (19 mm), and 1 in (25 mm).

5. Reduced embedded length for low confined specimens, may result in full pullout testing and avoid premature failure due to splitting.

6. A local bond slip incorporating maximum aggregate size, cover and steel bar size, as well as the environmental condition, using data from suggested matrix testings could be a massive benefit in predicting bond-slip.

References

ACI Committee 408 (2003). Bond and development of straight reinforcing bars in tension (ACI 408R-03). *American Concrete Institute, Detroit, Michigan, US*, page 49. 6, 7, 9

Abrishami, H. G. and Mitchell, D. (1993). Bond characteristics of pretensioned strand. *Materials Journal*, 90(3):228–235. 10

ACI Committee and International Organization for Standardization (2019). Building code requirements for structural concrete (aci 318-19) and commentary. American Concrete Institute.

ASTM C39/C39M (2012). Standard test method for compressive strength of cylindrical concrete specimens. 32

ASTM Standard C127 (2015). Standard test method for relative density (specific gravity) and absorption of coarse aggregate. ASTM West Conshohocken, PA. 31, 32

ASTM Standard C128 (2015). Standard test method for relative density (specific gravity) and absorption of fine aggregate. ASTM West Conshohocken, PA. 31, 32

Darwin, D. and Graham, E. K. (1993). Effect of deformation height and spacing on bond strength of reinforcing bars. Technical report, University of Kansas Center for Research, Inc. 7

Darwin, D., Idun, E. K., Zuo, J., and Tholen, M. L. (1995). Reliability-based strength reduction factor for bond. Technical report, University of Kansas Center for Research, Inc. 7

Darwin, D., McCabe, S. L., Idun, E. K., and Schoenekase, S. P. (1992). Development length criteria: bars not confined by transverse reinforcement. American Concrete Institute. 7, 9

Eligehausen, R., Popov, E. P., and Bertero, V. V. (1982). Local bond stress-slip relationships of deformed bars under generalized excitations. 9

Fib, B. (2000). 10, bond of reinforcement in concrete, state of the art report prepared by task group bond models, former ceb, task group 5.2. *CH-1015*.

Filippou, F. C., Popov, E. P., and Bertero, V. V. (1983). Modeling of r/c joints under cyclic excitations. *Journal of Structural Engineering*, 109(11):2666–2684. 9

Grosse, C. U. (2007). *Advances in Construction Materials 2007*. Springer Berlin Heidelberg. 1

Hamad, B. S. and Itani, M. S. (1998). Bond strength of reinforcement in high performance concrete: role of silica fume, casting position, and superplasticizer dosage. *Materials Journal*, 95(5):499–511. 9, 44

Iqbal, S., Ullah, N., and Ali, A. (2018). Effect of maximum aggregate size on the bond strength of reinforcements in concrete. *Engineering, Technology & Applied Science Research*, 8(3):2892–2896. 9, 44

Lutz, L. A. and Gergely, P. (1967). Mechanics of bond and slip of deformed bars in concrete. In *Journal Proceedings*, volume 64, pages 711–721. 7

Maruyama, I., Kontani, O., Takizawa, M., Sawada, S., Ishikawao, S., Yasukouchi, J., Sato, O., Etoh, J., and Igari, T. (2017). Development of soundness assessment procedure for concrete members affected by neutron and gamma-ray irradiation. *Journal of Advanced Concrete Technology*, 15(9):440–523. 1, 12

Orangun, C., Jirsa, J., and Breen, J. (1977). A reevaulation of test data on development length and splices. In *Journal Proceedings*, volume 74, pages 114–122. 9

Rehm, G. and Eligehausen, R. (1979). Bond of ribbed bars under high cycle repeated loads. 7, 9

Skorobogatov, S. and Edwards, A. (1979). The influence of the geometry of deformed steel bars on their bond strength in concrete. *Proceedings of the Institution of Civil Engineers*, 67(2):327–339. 7

Tang, C.-W. (2021). Modeling uniaxial bond stress–slip behavior of reinforcing bars embedded in concrete with different strengths. *Materials*, 14(4):783. 10

Tennessee Department of Transportation (2021). Standard specifications for road and bridge construction.

Vázquez-Herrero, C., Martínez-Lage, I., Aguilar, G., and Martínez-Abella, F. (2013). Evaluation of strand bond properties along the transfer length of prestressed lightweight concrete members. *Engineering structures*, 49:1048–1058. 10

Walraven, J. et al. (2010). *Model Code 2010-First complete draft-Volume 1: Model Code*, volume 56. fib Fédération internationale du béton. 9

Zuo, J. and Darwin, D. (1998). Bond strength of high relative rib area reinforcing bars. Technical report, University of Kansas Center for Research, Inc. 9

Vita

Mohammed Abdelrahman was born in Sudan. He began studying at the University of Khartoum, Sudan in 2005 and graduated with a B.S. in Civil Engineering in 2010. He joined King Fahd University of Petroleum and Minerals, Saudi Arabia to pursue a M.S. in Civil Engineering and graduated in 2015. After a few years of working in the industry, he enrolled at the University of Tennessee, United States to earn a master's degree in civil engineering with a concentration in Structural Engineering. He plans to have a professional career as a structural engineer in industry.